

Switchable quantized signal between longitudinal conductance and Hall conductance in dual quantum spin Hall insulator TaIrTe₄

Junwen Lai,^{†,‡} Xiangyang Liu,^{†,‡} Jie Zhan,^{†,‡} Tianye Yu,[‡] Peitao Liu,^{†,‡} Xing-Qiu Chen,^{*,†,‡} and Yan Sun^{*,†,‡}

[†]*School of Materials Science and Engineering, University of Science and Technology of China, Shenyang 110016, China.*

[‡]*Shenyang National Laboratory for Materials Science, Institute of Metal Research, Chinese Academy of Sciences, Shenyang 110016, China.*

E-mail: xingqiu.chen@imr.ac.cn; sunyan@imr.ac.cn

Abstract

Topological insulating states in two-dimensional (2D) materials are ideal systems to study different types of quantized response signals due to their in gap metallic states. Very recently, the quantum spin Hall (QSH) effect was discovered in monolayer TaIrTe₄ via the observation of quantized longitudinal conductance that rarely exists in other 2D topological insulators. The non-trivial Z_2 topological charges can exist at both charge neutrality point and the van Hove singularity point with correlation effect induced band gap. Based on this model 2D material, we studied the switch of quantized signals between longitudinal conductance and transversal Hall conductance via tuning external magnetic field. In Z_2 topological phase of monolayer TaIrTe₄, the zero Chern number can be understood as $1-1=0$ from the double band inversion from

spin-up and spin-down channels. After applying a magnetic field perpendicular to the plane, the Zeeman split changes the band order for one branch of the band inversion from spin-up and spin-down channels, along with a sign change of the Berry phase. Then the net Chern number of $1-1=0$ is tuned to $1+1=2$ or $-1-1=-2$ depending on the orientation of the magnetic field. The quantized signal not only provides another effective method for the verification of topological state in monolayer TaIrTe₄, but also offers a strategy for the utilization of the new quantum topological states based on switchable quantized responses.

Introduction and motivation

Topological states in two-dimensional (2D) systems have been extensively studied in the last decades. The quantum Hall (QH) effect is the first discovered topological state in materials, which presents as quantized Hall conductance in the unit of e^2/h with zero longitudinal resistance.¹⁻⁴ The quantized Hall conductance originated from the dissipative chiral edge state, while all the other states are localized. In electronic band structures, the occupied and non-occupied states are connected by the chiral edge states located in the bulk band gap. The number of net edge channels can be understood from the Chern number of bulk band structures. Since the Hall conductance in the QH effect is only dependent on the fundamental constant of the electron charge and the Planck constant, it plays an important role in the metrology resistance standards and quantum computing.⁵⁻⁸

In history, most of the QH effect states were measured in 2D electron gas under strong perpendicular magnetic fields.⁹⁻¹⁴ With the generalization of topological band theory in condensed matter physics, it is found that different types of topological states exist in nature and applied magnetic fields can control different topological phase transitions, including both insulating and semimetal states. With this guiding principle, the QH effect and quantum anomalous Hall (QAH) effect were realized in topological insulators and the thin film of Dirac semimetals,¹⁵⁻²⁸ and the QH effect is even generalized into three-dimensional (3D)

electron systems.^{29–34}

The interplay between the magnetic field and 2D topological materials provides an ideal platform for the study of topological phase transition among quantum spin Hall (QSH) insulators, topological semimetal, QH effect, and QAH effect et al.^{35–37} In addition to plenty of quantum topological phases, the topological phase transition also offers an effective approach for detecting the topological states from quantized transport signals. Very recently, TaIrTe₄ monolayer was experimentally fabricated and confirmed as a new dual QSH insulator.³⁸ The nontrivial Z_2 topological charges in TaIrTe₄ exist at both the charge neutrality point and the van Hove singularity point with a new band gap induced by strong correlations. Owing to its 2D nature, monolayer TaIrTe₄ can be understood as a model material for realizing different types of topological states under perturbations of strain, gating, magnetic field, and magnetic doping et al.

In this work, we studied the evolution of magnetic field-induced topological phase transition from Z_2 QSH insulator to QH insulator. Along with these phase transitions, the quantized signals of longitudinal conductance and Hall conductance are switched on and off via the control of an external magnetic field, as schematic shown in Fig. 1. The topological phase transition provides an effective approach to obtain a QH effect state starting from the time-reversal symmetry 2D topological insulators, and the switchable quantized signals offer a strategy for the utilization of the new quantum topological material.

Result and Discussion

Bulk TaIrTe₄ is a well known typical type-II Weyl semimetal which crystallized by an AB stacking of two centrosymmetric van-der waals layers.^{39,40} Its monolayer was theoretically predicted as a QSH insulator at the charge neutrality point and very recently experimentally verified by the observation of quantized longitudinal conductance.^{38,41} In addition, the correlation effect induced a nontrivial Z_2 band gap also existed when weakly doping shifted

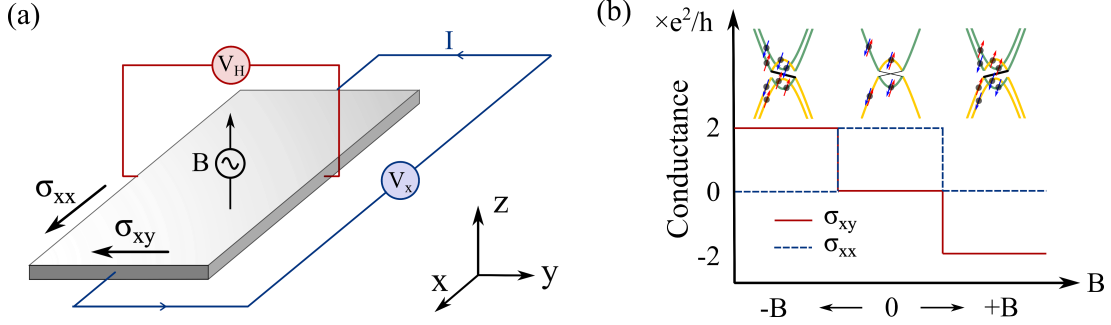


Figure 1: Schematic illustration of the magnetic field-induced conductance change under topological phase transition. (a) Illustration of the longitude(σ_{xx}) and Hall(σ_{xy}) conductance under a varying perpendicular magnetic field B , the input current I is along the x direction. (b) Topological phase transition induced conductance (σ_{xx}, σ_{xy}) change under a varying perpendicular magnetic field B , the yellow and green colors stand for the different orbitals, the red and blue arrows on the band structure represents the spin up and down states, respectively.

the Fermi level to the van Hove singularity points.³⁸The monolayer TaIrTe_4 crystallized in a space group of $P2_1/m$ (No.11) which consists of two symmetry operators of inversion i and $\{C_{2y}|(0, 1/2, 0)\}$, see Fig. 2.

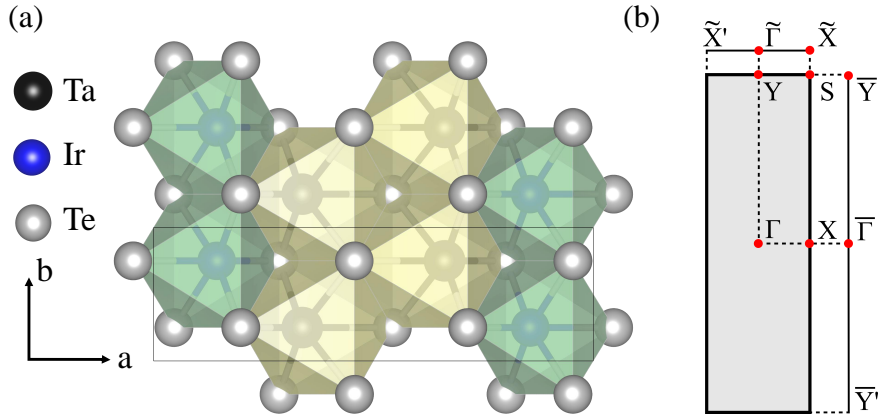


Figure 2: Crystal lattice structure and Brillouin zone of monolayer TaIrTe_4 . (a) Top view of monolayer TaIrTe_4 (b) Brillouin zone and its projection to different direction $[100]$ and $[010]$ of monolayer TaIrTe_4

Based on the experimental reported lattice structure³⁹, the electronic band structures evolution of TaIrTe_4 is calculated with a tuning external magnetic field. As presented in Fig. 3(a), in the condition without external field, there is a band inversion at X point between the conduction and valence band with a band gap of ~ 24 meV, which can be seen from the

“W-shape” of the dispersion near the bottom of conduction bands, in good agreement with previous reports.^{41,42} The Z_2 topological feature can be directly confirmed by the Wannier center evolution. From Fig. 3(a), one can easily see that the evolution of Wannier centers in $k_1 - k_2$ plane presents as a zigzag form with changing partners at the time-reversal invariant point. Hence, the evolution lines cross the reference line an odd number of times in the half Brillouin zone (BZ).

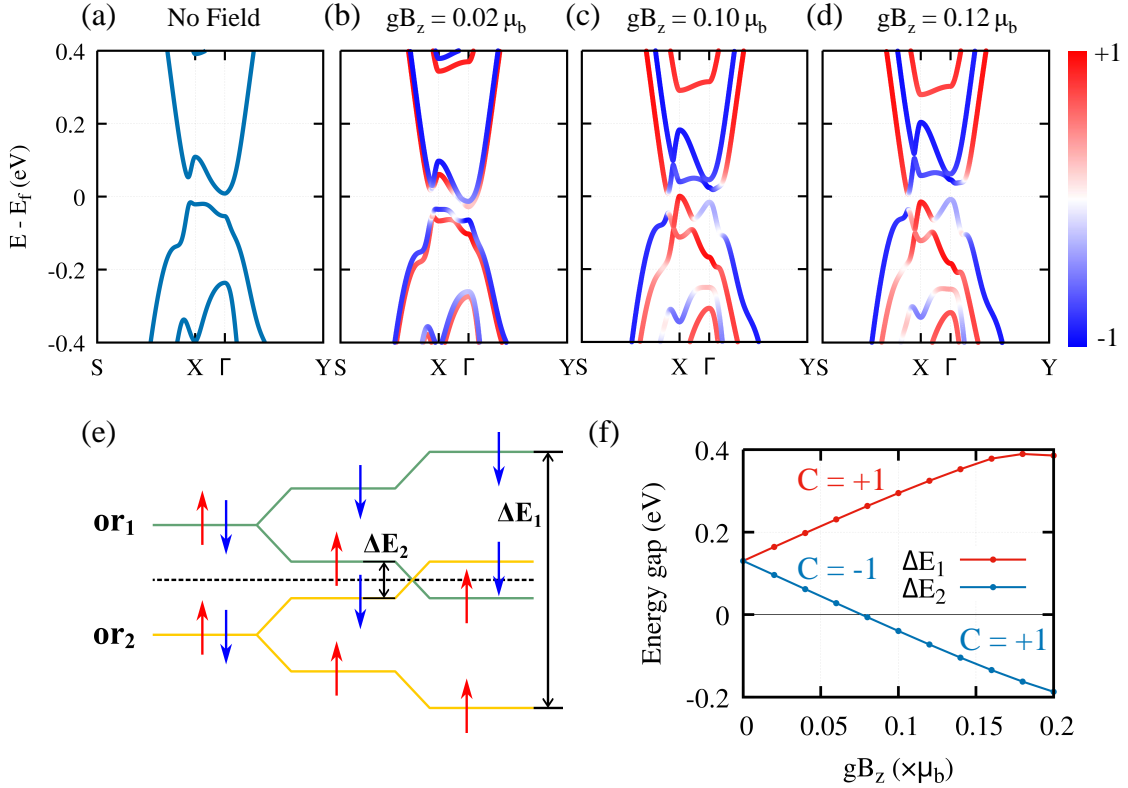


Figure 3: Evolution of electronic band structure and topological numbers of monolayer TaIrTe₄ under magnetic field. (a) The band structure without magnetic field. (b-d) The spin-resolved band structures under different gB_z . The red and blue colors represent the z component of spin channels. (e) Schematic diagram of the band inversion progress at X point with an increasing Zeeman field, the green and yellow lines stand for the different orbitals near Fermi energy, namely or_1 , and or_2 , the red and blue arrows stand for the spin states. $\Delta E_1 = E_{or_1-down} - E_{or_2-up}$ and $\Delta E_2 = E_{or_1-up} - E_{or_2-down}$ are energy differences between the spin up(down) state of or_1 and spin down(up) state of or_2 . (f) The energy change of ΔE_1 (ΔE_2) at high symmetry point of X under an increasing magnetic field gB_z . ΔE_1 states at positive zone in the whole progress, with a constant Chern number 1. ΔE_2 changes sign at around $gB_z = 0.08 \mu_B$, along with the change of Chern number from -1 to 1.

The magnetic field serves as an effective way to tune the electronic band structure and band order, as it breaks the time-reversal symmetry. We try to apply an external magnetic field perpendicular to the monolayer TaIrTe₄, see the sketch in Fig. 1(a). As long as a non-zero magnetic field is introduced, the degeneracy of spin-up and spin-down is broken and an obvious Zeeman split could be observed in both valence and conduction bands, see Fig. 3(b). Correspondingly, the time-reversal symmetry of Wannier center evolution is broken compared to the non-field state and the positive and negative parts along k_1 are not equal anymore, see Fig. 4(a-b).

As the magnetic field increases, the Zeeman split gets larger. In addition to the band spin split, we can see that the spin-up and spin-down channels move in opposite directions in energy space, as the comparison between Fig. 3(b-d). In this mechanism, the original band inversion from orbital1-spin-down and orbital2-spin-up channels remain unchanged, only with the magnitude of the inverted band gap increasing. On the other hand, the spin-up channel from orbital1 moves down, and the spin-down channel from orbital2 moves up, a new band inversion from orbital1-spin-up and orbital2-spin-down happens, see the schematic diagram in Fig. 3(e).

From band number indexed Berry phase calculations, we found that the original band inversion due to crystal field and spin-orbital coupling, i.e. the band inversion between orbital1-spin-down and orbital2-spin-up, hosts a Chern number 1. Similarly, the original band inversion between orbital1-spin-up and orbital2-spin-down hosts a Chern number -1. Hence, in the case of nontrivial Z_2 state and with a weak Zeeman field, the net Chern number is 0. On the other hand, the newly generated band inversion between orbital1-spin-up and orbital2-spin-down induced from the magnetic field has a Chern number 1. Consequently, the new phase with Zeeman field above $0.1\mu_B$ has a none zero quantized Hall conductance of $2e^2/h$.

The evolution of band gaps between different orbital and spin characters, i.e. $\Delta E_1 = E_{or1-down} - E_{or2-up}$ and $\Delta E_2 = E_{or1-up} - E_{or2-down}$, is given in Fig. 3(f). We can see that

the positive band gap of ΔE_2 decreases to zero at around $gB_z = 0.08 \mu_B$ and then goes to the negative zone. Correspondingly, the Chern number between orbital1-spin-up and orbital2-spin-down changes from -1 to 1. On the other hand, the band gap of ΔE_1 follows the opposite trend. It keeps staying at the positive zone and shares the same trend with the increasing of magnetic field up to $0.12 \mu_B$, with a constant Chern number 1 in the whole process. Therefore, the topological phase transition is mainly induced by the band order between orbital1-spin-up and orbital2-spin-down. The sign change of Chern number from -1 to 1 for the band gap of ΔE_2 leads to a net Chern number 2 for the whole system.

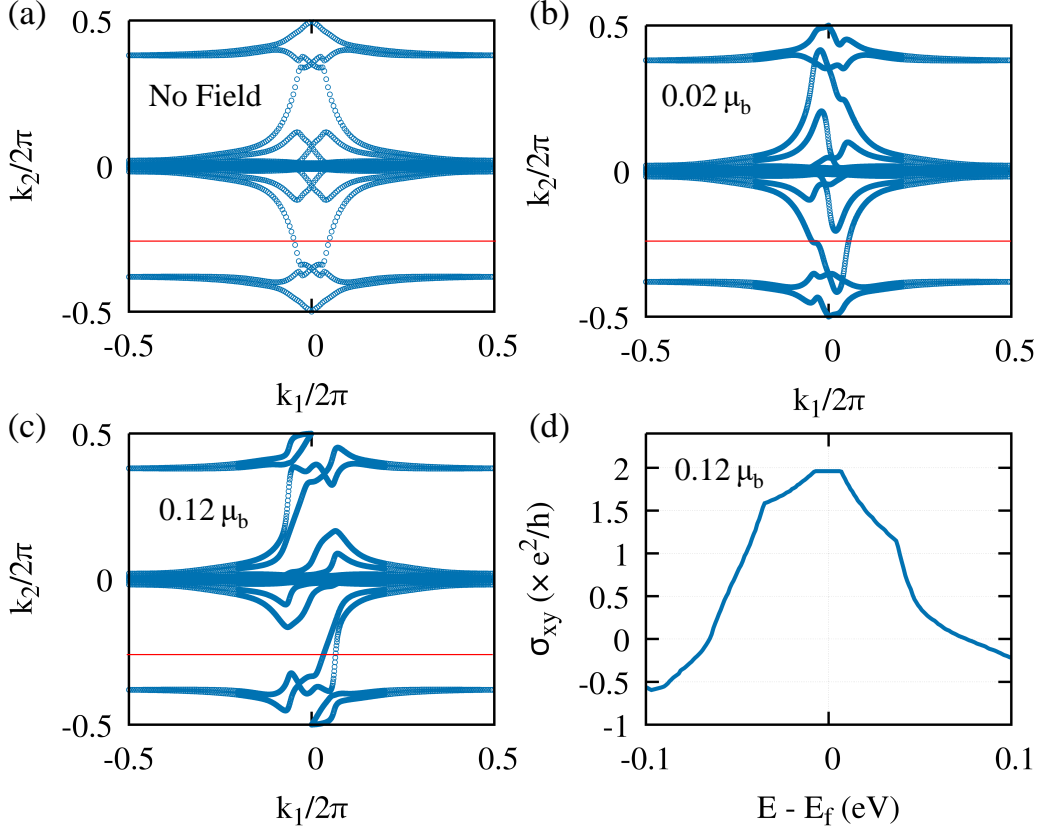


Figure 4: Wannier center evolution in different conditions. (a-c) Wannier center evolution under different magnetic fields. (d) Anomalous hall conduct of the QH state in the unit of e^2/h under different chemical potentials.

The QH insulating state was also confirmed by the Wannier center evolution in the 2D BZ at the magnetic field of $gB_z = 0.12 \mu_B$. As presented in Fig. 4(c), with time-reversal symmetry breaking, the evolution of Wannier center evolves in the whole range of k_1 axis.

When fixing the band number n as the fully occupied states, the Wannier center evolution lines cross the reference line twice, where both of the two evolution lines show a positive slope. From the energy dispersion in Fig. 3(d), we can see a global band gap around 14 meV, so a quantized Hall conductance is expected. We then further calculated the chemical potential dependent Hall conductance by following the linear response Kubo formula approach, see the method part for details. From Fig. 4(d), we can see a stable plateau of $2e^2/h$ near the charge neutrality point at the situation of $gB_z = 0.12 \mu_B$, fully in agreement with the band indexed Berry phase analysis and Wilson loop calculations. Based on the above analysis, we tried to rotate the magnetic field to the $-z$ direction and found that both the slope of Wannier center evolutions and Hall conductance change the signs.

For both QSH insulators and QH insulators, the quantized signals originate from the edge states located inside the bulk band gaps. Fig. 5(a) is the projected edge states for the QSH insulator phase along $\bar{Y} - \bar{\Gamma} - \bar{Y}$, with spin helical linear crossing edge Dirac point locating at $\bar{\Gamma}$. As long as a z -oriented magnetic field is applied, the Dirac point is broken by opening an anti-crossing-like band gap, due to time-reversal symmetry breaking, see Fig. 5(b). After the new band inversion happens between orbital1-spin-up and orbital2-spin-down at X point, the spin helical edge states transfer to chiral edge states with positive velocity connecting the occupied and non-occupied bulk bands, see Fig. 5(c-d). Though the specific shapes of the edge states are dependent on the details of edge potentials, the net crossing points between the chiral edge states and Fermi levels are both 2 for the open boundary condition along x and y directions, fully consistent with the bulk topological charge analysis. Therefore, the quantized signals are switchable between longitudinal conductance and transversal Hall conductance, via tuning the external magnetic field.

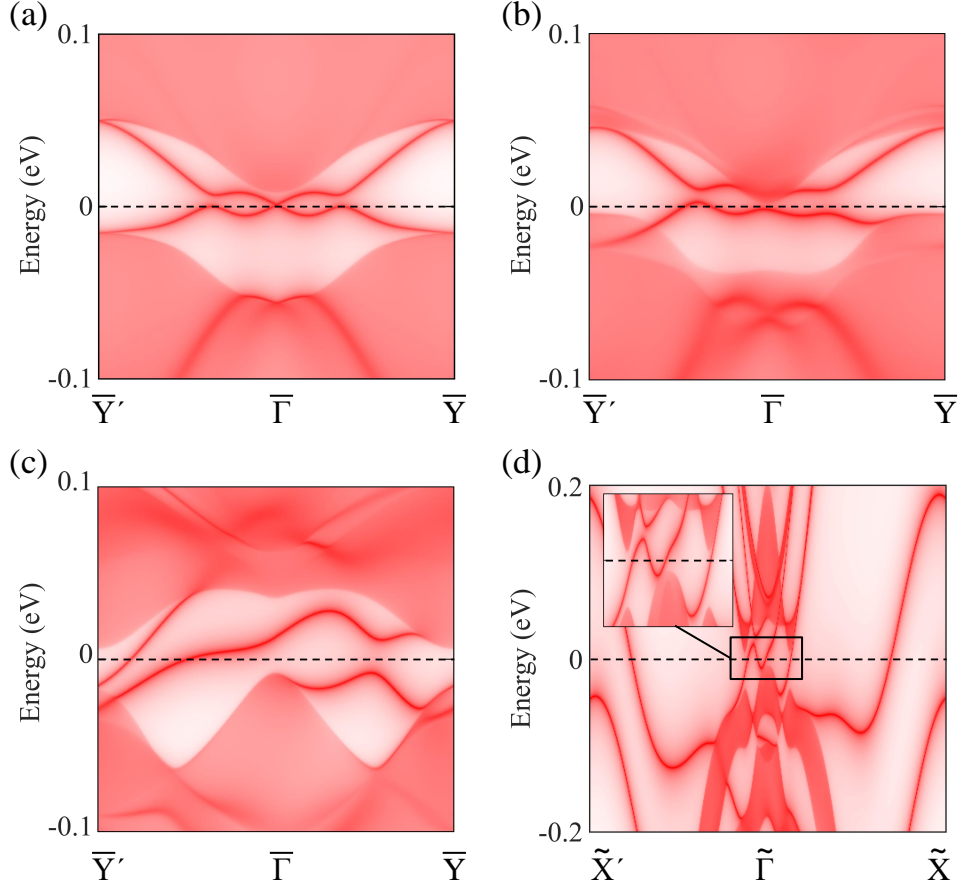


Figure 5: Projected edge states in different situations for monolayer TaIrTe₄ with and without magnetic field. (a) [010] surface without magnetic field. (b) [010] surface with $gB_z = 0.02 \mu_B$. (c) [010] surface with $gB_z = 0.12 \mu_B$. (d) [100] surface with $gB_z = 0.12 \mu_B$. The inset in (d) is an enlarged surface states near $\tilde{\Gamma}$. The other edge states away from $\tilde{\Gamma}$ could be attributed to the topological order of intra-valance bands.

Conclusion

In summary, we studied magnetic field-induced topological phase transition in the newly discovered dual QSH insulator TaIrTe₄. Applying a magnetic field along z -direction, the original band order of the inverted band gap from one branch of the spin-up and spin-down channels is exchanged, with the corresponding Chern number transferring from -1 to 1. Together with another original branch of band inversion with Chern number 1, the topological phase transition happens between the QSH insulator and the QH insulator. Since the QSH insulator state in monolayer TaIrTe₄ can host a non-zero quantized longitudinal

conductance that rarely exists in other 2D Z_2 topological insulators, such topological phase transition is along with the exchange of quantized signals between longitudinal conductance and transversal Hall conductance. This result also proposes another effective strategy to verify the existence of QSH insulating state in TaIrTe₄.

Method

Ground state study of monolayer TaIrTe₄ and the Wannier projection is carried out in Full-Potential Local-Orbital(FPLO) package under generalized gradient approximation (GGA) with Perdew-Burke-Ernzerhof (PBE) parametrization.⁴³⁻⁴⁵ Self-consistent energy reaches a convergence of 10^{-6} eV. Structure from the experimental is applied with lattice constants of $a = 12.42 \text{ \AA}$ and $b = 3.77 \text{ \AA}$, a vacuum of 15 \AA is applied on c axis to eliminate the inter-layer interaction. Magnetic field is simulated by adding Zeeman splitting Hamiltonian on Wannier basis H_0 which reads $H = H_0 + H_Z$, where $H_Z = g\mathbf{B} \cdot \boldsymbol{\sigma}$. For out-of-plane magnetic field $\mathbf{B} \parallel z$, it could be written as a scalar $H_Z = gB_z\sigma_z$. Based on H , edge states calculation is performed by the iteration of green function⁴⁶ while the wannier center evolution is carried out by the Wilson loop method.⁴⁷ Anomalous hall conductivity with varying chemical potential is performed by Kubo formula⁴⁸ in clean limit

$$\sigma_{xy}(E) = \frac{e^2}{\hbar S} \int [d\mathbf{k}] \sum_i f^i(E, \mathbf{k}) \Omega_{xy}^i(\mathbf{k})$$

$$\Omega_{xy}^i(\mathbf{k}) = \sum_j \text{Im}\{r_x^{ij}(\mathbf{k}), r_y^{ji}(\mathbf{k})\}$$
(1)

whereas $r_a^{ij}(\mathbf{k}) = i \langle u_i(\mathbf{k}) | \partial_{k_a} | u_j(\mathbf{k}) \rangle$, $|u_i(\mathbf{k})\rangle$ represents the i^{th} Wannier state, S is the in-plane area of monolayer TaIrTe₄, $H_{ij}(\mathbf{k})$ is the Hamiltonian of the system while $f^i(E, \mathbf{k})$ is the occupation of band index i with momenta \mathbf{k} under a chemical potential E . For the numerical integration over BZ, a k -point sampling of $6 \times 18 \times 1$ is applied for the ground state DFT study while a sampling of $2000 \times 2000 \times 1$ is used for the anomalous hall conductivity

calculation.

Acknowledgement

This work was supported by the National Key R&D Program of China (Grant No. 2021YFB3501503), the National Natural Science Foundation of China (Grants No. 52271016 and No. 52188101), and Foundation from Liaoning Province (Grant No. XLYC2203080). Part of the numerical calculations in this study were carried out on the ORISE Supercomputer.

References

- (1) Laughlin, R. B. Quantized Hall Conductivity in Two Dimensions. *Phys. Rev. B* **1981**, *23*, 5632–5633.
- (2) Tsui, D. C.; Stormer, H. L.; Gossard, A. C. Two-Dimensional Magnetotransport in the Extreme Quantum Limit. *Phys. Rev. Lett.* **1982**, *48*, 1559–1562.
- (3) Thouless, D. J.; Kohmoto, M.; Nightingale, M. P.; den Nijs, M. Quantized Hall Conductance in a Two-Dimensional Periodic Potential. *Phys. Rev. Lett.* **1982**, *49*, 405–408.
- (4) Tsukazaki, A.; Ohtomo, A.; Kita, T.; Ohno, Y.; Ohno, H.; Kawasaki, M. Quantum Hall Effect in Polar Oxide Heterostructures. *Science* **2007**, *315*, 1388–1391.
- (5) Hasan, M. Z.; Kane, C. L. Colloquium: Topological Insulators. *Rev. Mod. Phys.* **2010**, *82*, 3045–3067.
- (6) Xiao, D.; Chang, M.-C.; Niu, Q. Berry Phase Effects on Electronic Properties. *Rev. Mod. Phys.* **2010**, *82*, 1959–2007.
- (7) Qi, X.-L.; Zhang, S.-C. Topological Insulators and Superconductors. *Rev. Mod. Phys.* **2011**, *83*, 1057–1110.

- (8) Sinova, J.; Valenzuela, S. O.; Wunderlich, J.; Back, C. H.; Jungwirth, T. Spin Hall Effects. *Rev. Mod. Phys.* **2015**, *87*, 1213–1260.
- (9) Cooper, J. R.; Kang, W.; Auban, P.; Montambaux, G.; Jérôme, D.; Bechgaard, K. Quantized Hall Effect and a New Field-Induced Phase Transition in the Organic Superconductor (TMTSF)₂PF₆. *Phys. Rev. Lett.* **1989**, *63*, 1984–1987.
- (10) Chu, H. T.; Henriksen, P. N.; Jing, J.; Wang, H.; Xu, X. Magnetic-Field Dependence of Hall Resistance in Thin Films of Pure Bismuth. *Phys. Rev. B* **1992**, *45*, 11233–11237.
- (11) Jiang, H. W.; Johnson, C. E.; Wang, K. L.; Hannahs, S. T. Observation of Magnetic-Field-Induced Delocalization: Transition from Anderson Insulator to Quantum Hall Conductor. *Phys. Rev. Lett.* **1993**, *71*, 1439–1442.
- (12) Liu, C.-X.; Qi, X.-L.; Dai, X.; Fang, Z.; Zhang, S.-C. Quantum Anomalous Hall Effect in Hg_{1-y}Mn_yTe Quantum Wells. *Phys. Rev. Lett.* **2008**, *101*, 146802.
- (13) Maciejko, J.; Hughes, T. L.; Zhang, S.-C. The Quantum Spin Hall Effect. *Annual Review of Condensed Matter Physics* **2011**, *2*, 31–53.
- (14) Feng, Y.; Feng, X.; Ou, Y.; Wang, J.; Liu, C.; Zhang, L.; Zhao, D.; Jiang, G.; Zhang, S.-C.; He, K.; Ma, X.; Xue, Q.-K.; Wang, Y. Observation of the Zero Hall Plateau in a Quantum Anomalous Hall Insulator. *Phys. Rev. Lett.* **2015**, *115*, 126801.
- (15) Yu, R.; Zhang, W.; Zhang, H.-J.; Zhang, S.-C.; Dai, X.; Zhong Fang Quantized Anomalous Hall Effect in Magnetic Topological Insulators. *Science* **2010**, *329*, 61–64.
- (16) Apalkov, V. M.; Chakraborty, T. Interacting Dirac Fermions on a Topological Insulator in a Magnetic Field. *Phys. Rev. Lett.* **2011**, *107*, 186801.
- (17) Zyuzin, A. A.; Hook, M. D.; Burkov, A. A. Parallel Magnetic Field Driven Quantum Phase Transition in a Thin Topological Insulator Film. *Phys. Rev. B* **2011**, *83*, 245428.

- (18) Beugeling, W.; Liu, C. X.; Novik, E. G.; Molenkamp, L. W.; Morais Smith, C. Reentrant Topological Phases in Mn-doped HgTe Quantum Wells. *Phys. Rev. B* **2012**, *85*, 195304.
- (19) Liu, X.; Hsu, H.-C.; Liu, C.-X. In-Plane Magnetization-Induced Quantum Anomalous Hall Effect. *Phys. Rev. Lett.* **2013**, *111*, 086802.
- (20) Zhang, J.; Chang, C.-Z.; Tang, P.; Zhang, Z.; Feng, X.; Li, K.; Wang, L.-l.; Chen, X.; Liu, C.; Duan, W.; He, K.; Xue, Q.-K.; Ma, X.; Yayu Wang Topology-Driven Magnetic Quantum Phase Transition in Topological Insulators. *Science* **2013**, *339*, 1582–1586.
- (21) Bahari, M.; Hosseini, M. V. Zeeman-Field-Induced Nontrivial Topological Phases in a One-Dimensional Spin-Orbit-Coupled Dimerized Lattice. *Phys. Rev. B* **2016**, *94*, 125119.
- (22) Chang, C.-Z.; Zhao, W.; Li, J.; Jain, J. K.; Liu, C.; Moodera, J. S.; Chan, M. H. W. Observation of the Quantum Anomalous Hall Insulator to Anderson Insulator Quantum Phase Transition and Its Scaling Behavior. *Phys. Rev. Lett.* **2016**, *117*, 126802.
- (23) Uchida, M.; Nakazawa, Y.; Nishihaya, S.; Akiba, K.; Kriener, M.; Kozuka, Y.; Miyake, A.; Taguchi, Y.; Tokunaga, M.; Nagaosa, N.; Tokura, Y.; Kawasaki, M. Quantum Hall States Observed in Thin Films of Dirac Semimetal Cd_3As_2 . *Nature Communications* **2017**, *8*, 2274.
- (24) Asaba, T.; Wang, Y.; Li, G.; Xiang, Z.; Tinsman, C.; Chen, L.; Zhou, S.; Zhao, S.; Laleyan, D.; Li, Y.; Mi, Z.; Li, L. Magnetic Field Enhanced Superconductivity in Epitaxial Thin Film WTe_2 . *Scientific Reports* **2018**, *8*, 6520.
- (25) Zhang, J.; Liu, Z.; Wang, J. In-Plane Magnetic-Field-Induced Quantum Anomalous Hall Plateau Transition. *Phys. Rev. B* **2019**, *100*, 165117.
- (26) Satake, Y.; Shiogai, J.; Mazur, G. P.; Kimura, S.; Awaji, S.; Fujiwara, K.; Nojima, T.; Nomura, K.; Souma, S.; Sato, T.; Dietl, T.; Tsukazaki, A. Magnetic-Field-Induced

- Topological Phase Transition in Fe-doped $(\text{Bi,Sb})_2\text{Se}_3$ Heterostructures. *Phys. Rev. Mater.* **2020**, *4*, 044202.
- (27) Kubisa, M.; Ryczko, K. Topological Phase Transitions and a Spin-Related Metallic State in Inverted HgTe Quantum Wells under in-Plane Magnetic Field. *Phys. Rev. B* **2021**, *104*, L161406.
- (28) Guo, B.; Miao, W.; Huang, V.; Lygo, A. C.; Dai, X.; Stemmer, S. Zeeman Field-Induced Two-Dimensional Weyl Semimetal Phase in Cadmium Arsenide. *Phys. Rev. Lett.* **2023**, *131*, 046601.
- (29) Tang, F.; Ren, Y.; Wang, P.; Zhong, R.; Schneeloch, J.; Yang, S. A.; Yang, K.; Lee, P. A.; Gu, G.; Qiao, Z.; Zhang, L. Three-Dimensional Quantum Hall Effect and Metal–Insulator Transition in ZrTe_5 . *Nature* **2019**, *569*, 537–541.
- (30) Galeski, S. et al. Unconventional Hall Response in the Quantum Limit of HfTe_5 . *Nature Communications* **2020**, *11*, 5926.
- (31) Li, H.; Liu, H.; Jiang, H.; Xie, X. C. 3D Quantum Hall Effect and a Global Picture of Edge States in Weyl Semimetals. *Phys. Rev. Lett.* **2020**, *125*, 036602.
- (32) Li, S.; Wang, C. M.; Du, Z. Z.; Qin, F.; Lu, H.-Z.; Xie, X. C. 3D Quantum Hall Effects and Nonlinear Hall Effect. *npj Quantum Materials* **2021**, *6*, 96.
- (33) Liu, J. Y. et al. Spin-Valley Locking and Bulk Quantum Hall Effect in a Noncentrosymmetric Dirac Semimetal BaMnSb_2 . *Nature Communications* **2021**, *12*, 4062.
- (34) Li, S.; Wang, C. M.; Du, Z. Z.; Qin, F.; Lu, H.-Z.; Xie, X. C. 3D Quantum Hall Effects and Nonlinear Hall Effect. *npj Quantum Materials* **2021**, *6*, 96.
- (35) Kawamura, M.; Mogi, M.; Yoshimi, R.; Tsukazaki, A.; Kozuka, Y.; Takahashi, K. S.; Kawasaki, M.; Tokura, Y. Topological Quantum Phase Transition in Magnetic Topological Insulator upon Magnetization Rotation. *Phys. Rev. B* **2018**, *98*, 140404.

- (36) Zhan, F.; Ning, Z.; Gan, L.-Y.; Zheng, B.; Fan, J.; Wang, R. Floquet Valley-Polarized Quantum Anomalous Hall State in Nonmagnetic Heterobilayers. *Phys. Rev. B* **2022**, *105*, L081115.
- (37) Kong, X.; Luo, W.; Li, L.; Yoon, M.; Berlijn, T.; Liang, L. Floquet Band Engineering and Topological Phase Transitions in 1T' Transition Metal Dichalcogenides. *2D Materials* **2022**, *9*, 025005.
- (38) Tang, J. et al. Dual Quantum Spin Hall Insulator by Density-Tuned Correlations in TaIrTe₄. *Nature* **2024**,
- (39) Mar, A.; Jobic, S.; Ibers, J. A. Metal-Metal vs Tellurium-Tellurium Bonding in WTe₂ and Its Ternary Variants TaIrTe₄ and NbIrTe₄. *Journal of the American Chemical Society* **1992**, *114*, 8963–8971.
- (40) Kumar, D.; Hsu, C.-H.; Sharma, R.; Chang, T.-R.; Yu, P.; Wang, J.; Eda, G.; Liang, G.; Yang, H. Room-Temperature Nonlinear Hall Effect and Wireless Radiofrequency Rectification in Weyl Semimetal TaIrTe₄. *Nature Nanotechnology* **2021**, *16*, 421–425.
- (41) Guo, P.-J.; Lu, X.-Q.; Ji, W.; Liu, K.; Lu, Z.-Y. Quantum Spin Hall Effect in Monolayer and Bilayer TaIrTe₄. *Phys. Rev. B* **2020**, *102*, 041109.
- (42) Zhao, L.; Yu, G.; Huang, X.; Chen, W. TaIrTe₄ Monolayer with Topological Insulator Characteristic: A New and Highly Efficient Electrocatalyst toward Oxygen Reduction Reaction. *J. Phys. Chem. C* **2022**, *126*, 19685–19692.
- (43) Opahle, I.; Koepnik, K.; Eschrig, H. Full-Potential Band-Structure Calculation of Iron Pyrite. *Phys. Rev. B* **1999**, *60*, 14035–14041.
- (44) Koepnik, K.; Eschrig, H. Full-Potential Nonorthogonal Local-Orbital Minimum-Basis Band-Structure Scheme. *Phys. Rev. B* **1999**, *59*, 1743–1757.

- (45) Koepernik, K.; Janson, O.; Sun, Y.; van den Brink, J. Symmetry-Conserving Maximally Projected Wannier Functions. *Phys. Rev. B* **2023**, *107*, 235135.
- (46) M P Lopez Sancho; J M Lopez Sancho; J Rubio Quick Iterative Scheme for the Calculation of Transfer Matrices: Application to Mo (100). *Journal of Physics F: Metal Physics* **1984**, *14*, 1205.
- (47) Yu, R.; Qi, X. L.; Bernevig, A.; Fang, Z.; Dai, X. Equivalent Expression of Z_2 Topological Invariant for Band Insulators Using the Non-Abelian Berry Connection. *Phys. Rev. B* **2011**, *84*, 075119.
- (48) Nagaosa, N.; Sinova, J.; Onoda, S.; MacDonald, A. H.; Ong, N. P. Anomalous Hall Effect. *Rev. Mod. Phys.* **2010**, *82*, 1539–1592.